JOURNAL OF GEOPHYSICAL RESEARCH, VOL. 107, NO. D15, 10.1029/2001JD001230, 2002

Climatic effects of an impact-induced equatorial debris ring

Peter J. Fawcett
Department of Earth and Planetary Sciences, University of New Mexico, Albuquerque, New Mexico, USA

Mark B. E. Boslough
Sandia National Laboratories, Albuquerque, New Mexico, USA

Received 16 August 2001; revised 9 January 2002; accepted 16 January 2002; published 3 August 2002.

[1] Several theoretical and laboratory studies suggest that some large impact events are capable of inserting material into space depending on mechanics of the impact. This material would quickly coalesce to form a temporary debris ring in orbit around the equator, which would cast its shadow on the winter hemisphere. The results of an atmospheric general circulation model (GCM) simulation where an orbiting equatorial debris ring is applied as a boundary condition to the model show how the longer-term effects of a major impact could affect the climate system. The primary effect is a severe cooling in the tropics and the subtropics, especially under the seasonally migrating ring shadow. The globe cools and becomes drier, with the exception of monsoonal regions that become wetter. The Hadley cell is weakened resulting in drier tropics and weaker subtropical high-pressure cells in the winter hemisphere. Because the tropics cool more than middle latitude regions, the equator-to-pole temperature gradient becomes shallower resulting in weaker tropospheric winds and less high-latitude storminess. We suggest that the late Eocene impact(s) (35.5 Ma) could have generated a geologically temporary orbiting debris ring based on the global distribution of tektites associated with these events and patterns of climate change immediately above the iridium/microtektite layer. The Cretaceous-Tertiary boundary event, while larger, did not produce a debris ring. We also suggest that an opaque debris ring could have acted as the trigger to at least one episode of global glaciation during the Neoproterozoic. *INDEX TERMS:* 1620 Global Change: Climate dynamics (3309); 3210 Mathematical Geophysics: Modeling; 3319 Meteorology and Atmospheric Dynamics: General circulation; 6265 Planetology: Solar System Objects: Planetary rings; *KEYWORDS:* impact, planetary ring, paleoclimate, tektitkes, Eocene, snowball Earth

1. Introduction

[2] A growing body of evidence shows that the Earth has been subjected to numerous impacts by comets and asteroids throughout its history. Notable examples include Meteor Crater, Arizona, the buried Cretaceous/Tertiary Chixulub crater [*Hildebrand et al.*, 1991], a late Triassic chain of at least five coeval craters spread across several continents [*Spray et al.*, 1998], the Precambrian Sudbury basin and many more. The effects of the larger impact events on Earth's environment and climate have been the subjects of much speculation and research over the past two decades; much of it focused on the K-T boundary event. Proposed mechanisms for impact-related climate changes include aspects of atmospheric chemistry, aerosol production, and shock heating of the atmosphere [e.g., *Prinn and Fegley*, 1987; *D'Hondt et al.*, 1994] or a stratospheric dust cloud that blocks a significant fraction of insolation [e.g., *Covey et al.*, 1990, 1994; *Pollack et al.*, 1983; *Toon et al.*, 1982, 1997]. Both classes of effects are usually thought to be geologically transient and conditions rapidly returned to preimpact conditions.

[3] An alternative mechanism to be explored here is an impact generated, circum-equatorial debris ring. Such a ring would enhance and prolong the effects of a large impact on the climate system by casting a shadow in the winter hemisphere of the planet and greatly reducing subtropical insolation receipt. We examine the effects on climate of such a ring shadow with an atmospheric general circulation model. As a first and rather extreme sensitivity test, we use a fully opaque debris ring. This analysis can help to guide interpretation of the geologic record in the absence of a definitive oblique impact crater.

[4] The idea of a circum-equatorial orbiting ring affecting Earth's climate is not new, but has not been widely discussed in the literature. *Crowell* [1983] suggested that during times of low-latitude glaciations (e.g., the Neoproterozoic), the Earth might have had an ice ring similar to Saturn's, which blocked equatorial insolation. This idea has not received much credence, as it is unclear how an ice ring could form about the Earth and the intensity of radiation at the Earth's relatively close distance to the sun would quickly ablate the ring away. *O'Keefe* [1980a] suggested that a temporary Earth ring lasting between one and several

0148-0227/02/2001JD001230$09.00

million years and made of tektite material could explain the large climatic changes that occurred at the end of the Eocene. This idea was supported by the approximate coincidence in timing of a large tektite strewn field [*Glass and Zwart*, 1979] and botanical data that suggest a dramatic decrease in winter temperatures with little change in summer temperatures [*Wolfe*, 1978]. An equatorial ring would cast a shadow on the winter hemisphere and explain the observed pattern of cooling in the biological data. The tektites were assumed to be of cosmic origin, perhaps from lunar volcanoes [see *King*, 1980; *O'Keefe*, 1980b] some of which struck the Earth and some of which missed the Earth and were trapped in geocentric orbit. *King* [1980] challenged this idea because of a lack of known lunar rocks that are chemically suitable source materials for the tektites and suggested instead that these tektites are more similar in composition to North American tuffs and tuffaceous sediments of this age (i.e., probably produced by an impact event at the Eocene). *O'Keefe* [1985] has also suggested a tektite ring for the terminal Cretaceous event with the tektite material being derived from lunar volcanic eruptions. Clearly, the evidence accumulated since 1985 are much more supportive of a large impact at the K-T boundary.

[5] The tektite strewn fields are now generally considered to be material that has been ejected by bolide impacts [e.g., *Koeberl et al.*, 1996] and traveled through the atmosphere and possibly in orbit about the Earth. We therefore consider that if the Earth ever did have one or more episodes of a transient circum-equatorial ring, the most likely source of material for the ring is from a large bolide impact. *Schultz and Gault* [1990] suggested that such an event is possible given a low angle impact and a large enough impactor. Other work has suggested that ejection of impact debris into orbit is possible through hydrodynamic interactions [e.g., *Boslough and Crawford*, 1997; *Crawford et al.*, 1995].

1.1. Impact Events in the Geological Record

[6] The record of large impacts on Earth is rather poorly preserved owing to plate tectonic activity (subduction) and erosion [*McLaren and Goodfellow*, 1990], subsequent burial of an impact crater by younger sediments (e.g., the K-T boundary Chixulub structure [*Hildebrand et al.*, 1991]), and tectonic deformation (e.g., the Proterozoic Sudbury ring structure [*Melosh*, 1989]). Despite this, there are a few exceptionally well preserved impact structures found in the geological record. The most famous of these events is the Cretaceous-Tertiary boundary event that is associated with a major biological extinction. The diameter of the impacting body was estimated to be 10 km based on the global extent of the iridium-bearing clay layer [*Alvarez et al.*, 1980]. The actual crater site was discovered at Chicxculub, a 180 km diameter buried bowl structure in the Yucatan Peninsula, Mexico [*Hildebrand et al.*, 1991]. Evidence of other large impacts is found throughout Earth history, and some examples include a multiple impact event in the late Triassic [*Spray et al.*, 1998], the end of the Eocene [*Ganapathy*, 1984] and in the Pliocene [*Schultz et al.*, 1998].

[7] Rates of impact events through geologic time have been estimated from a variety of data. The cratering record of the other inner planets and the moon show that the early period of heavy bombardment ended around 3.8 Ga [e.g., *Barlow*, 1990] and that since then, large impacts have been less frequent. Estimates of impact rates in the Phanerozoic based on the Earth's cratering record and the number of asteroids and comets in Earth crossing orbits [*Shoemaker et al.*, 1988] range from one every 7 to 14 Myr for bolides with a diameter $\geq$5 km and one every 55 to 100 Myr for 10 km diameter bolides [*Shoemaker*, 1983; *McLaren and Goodfellow*, 1990].

[8] Clearly, large impacts must have affected the evolution of the Earth, life on it, and its atmospheric environment. Most work on the environmental effects of a large impact has been done for the K-T boundary event. A variety of studies suggest that ejection of material from the impact site into the atmosphere will result in the suspension of fine dust in the upper atmosphere blocking a significant fraction of sunlight [*Toon et al.*, 1982; *Pollack et al.*, 1983]. The climatic effects of such a stratospheric dust cloud have been investigated by *Covey et al.* [1990, 1994] and *Toon et al.* [1997]. The collective results of this work suggest an intense global cooling but not a global freeze event. Longer-term effects of large impacts are relatively unknown but some authors have suggested that they could cause tectonic and volcanic episodes [e.g., *Seyfert and Sirkin*, 1979; *Rampino and Stothers*, 1988].

1.2. Planetary Ring Formation via a (Low Angle) Impact Mechanism

[9] A growing body of evidence and experimental work suggests that large impact events are capable of ejecting some fraction of material into space, which could coalesce and form a geologically temporary debris ring. The global extent of the iridium-bearing clay layer and shocked quartz at the K-T boundary clearly demonstrates that material was ejected at near-orbital escape velocities following the impact event. A purely ballistic ejection that does not involve hydrodynamic interactions would not allow such particles to remain in orbit, and they would reenter the atmosphere and impact within one orbital period. However, hydrodynamic interactions among the solid debris, the atmosphere, and an expanding vapor cloud are increasingly being recognized as an important component of terrestrial impact physics and this could possibly provide the conditions that would lead to orbital trapping of debris.

[10] Theoretical calculations and laboratory experiments both show that under certain impacting conditions, planetary and impactor material can be inserted into orbit and can even escape Earth's gravity field. *O'Keefe and Ahrens* [1986] performed a series of calculations that showed the formation of high-velocity downrange vapor plumes for a range of oblique impact angles and sufficiently high impact velocities. These vapor plumes could be a mechanism for accelerating surface rocks to planetary escape velocities, and were cited as a means of propelling Martian origin rocks into space and ultimately to Earth [*O'Keefe and Ahrens*, 1986].

[11] A series of laboratory experiments have also demonstrated the possibility of injecting substantial amounts of material into orbit [*Schultz and Gault*, 1990]. At low impact angles (30° or less from the horizontal), the original impactor disrupts and ricochets downrange at a significant fraction of its incoming velocity. The ricochet component becomes embedded in and accelerated by an expanding

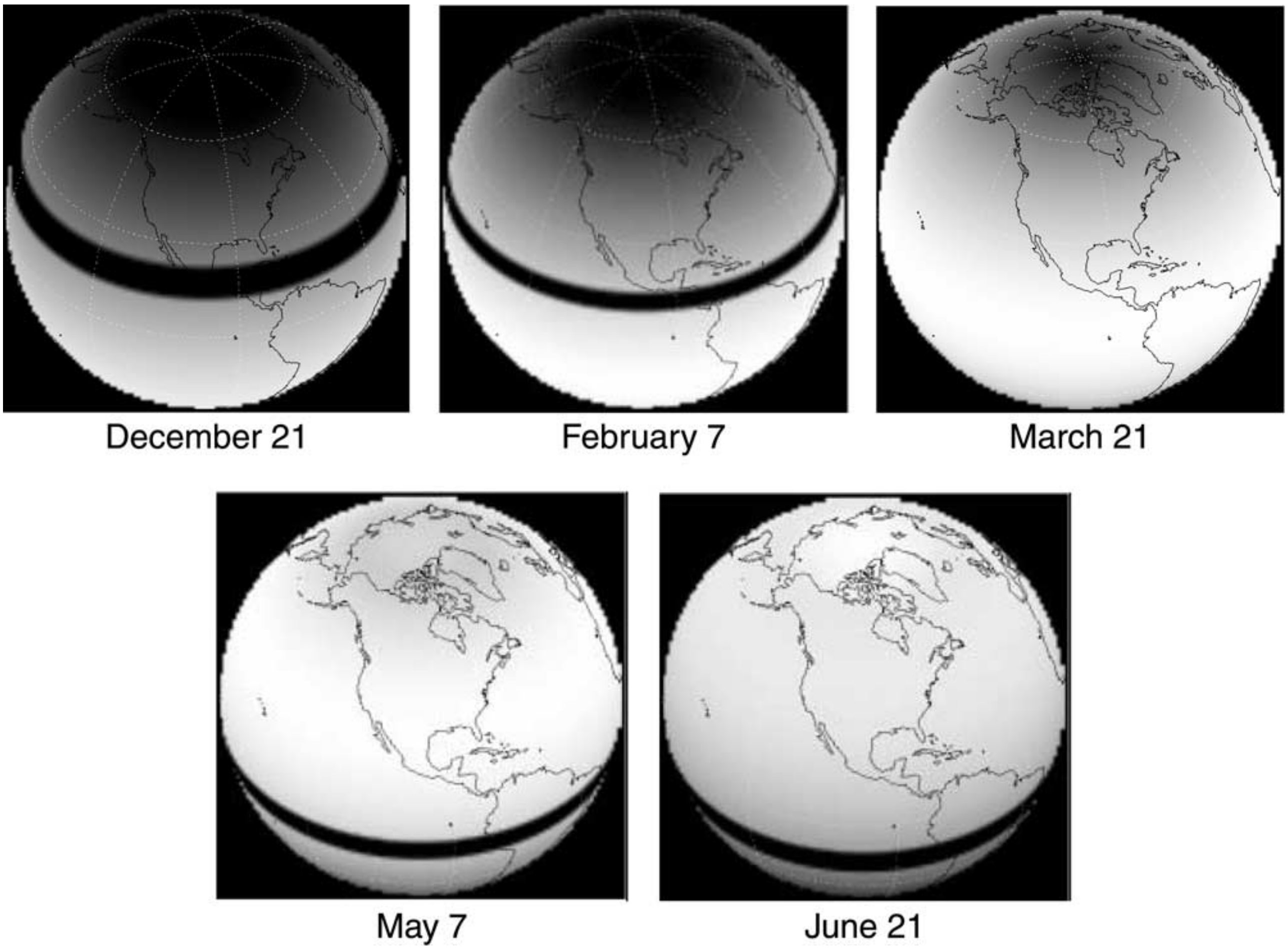

Figure 1. The seasonal migration of a subtropical insolation shadow caused by an equatorial debris ring in orbit around the Earth.

vapour cloud. Continued interaction between the solid debris and the turbulent expanding vapor cloud can potentially provide the nonballistic force that allows some fraction of the debris to be inserted into orbit. *Schultz and Gault* [1990] calculated that the optimum conditions for inserting a large mass of material into orbit would be for an oblique impact between 10° and 20° from the horizontal into an ocean or carbonate sediments with an incoming velocity between 15 and 20 km/s. For a 10-km-diameter body, the oblique impact event described above would be likely once every 300 million years [*Schultz and Gault*, 1990].

[12] An orbiting cloud of debris will collapse to a single plane within Earth's Roche limit by the same orbital mechanics that led to Saturn's and other planets' ring systems. Dynamical models of the development and evolution of disk formation predict a rapid ring development through collisional dampening [*Brahic*, 1977]. The stable location for such a planetary ring is the Laplacian plane, defined by the total angular momentum of the planetary system. Saturn is a rapidly rotating, low-density gas giant where the equatorial diameter is 10% greater than the polar diameter. For Earth, the mass of the moon competes with the equatorial bulge so the dynamically stable ring plane would lie between the equatorial plane and the lunar orbit plane (which precesses between 18° and 29° from the equatorial plane). For simplicity, we assume as a first approximation that any ring will lie in the equatorial plane.

1.3. Planetary Rings and Insolation

[13] An equatorial ring would cast a shadow primarily in the tropics, as is the case for Saturn. The location, surface area and darkness of the ring shadow would have a strong seasonal dependence, resulting in a net insolation reduction in the winter hemisphere (Figure 1). The maximum insolation loss would be during the solstices when the ring shadow is most extensive. At the equinoxes, the ring would be parallel to the subsolar direction and the shadow would be negligible.

[14] The radial extent and opacity of an equatorial ring would depend on a number of factors making it difficult to specify any one ring geometry and opacity as the most likely. The grain size, total amount, and optical properties of material inserted into orbit via impact would determine the opacity of the ring (for a given radial extent) and the complex orbital mechanics of a planetary ring in a system with one large moon would determine the radial extent of the ring. Given the main purpose of this work, which is to determine the possible first order effects of an equatorial ring system on the Earth's climate, we have chosen to represent the ring as an opaque, scaled Saturn B ring. Of

Saturn's three classical rings, the B ring is the optically thickest (opaque) and casts a shadow on Saturn's equator. It extends from a minimum radius, $r_{\min}$ of 1.53 Saturn radii to a maximum radius, $r_{\max}$ of 1.93 Saturn radii [*Cuzzi*, 1983]. Scaling these dimensions to Earth's radius (6378 km) gives an $r_{\min}$ of 9758 km and an $r_{\max}$ of 12,310 km. The inner edge of the ring would be 3380 km above the surface and the outer edge 5932 km above the surface for a total radial ring width of 2552 km. We have assigned an opacity of one to this ring, such that no light passes through it. This is only one of a multitude of possible ring parameters but as a sensitivity test for the effects of a planetary ring shadow on climate, it serves very well.

[15] The normal insolation pattern for an atmospheric general circulation model was modified by calculating the effects of the ring shadow on insolation. The ring itself lies well outside of the atmosphere and does not interact directly with it, so this scheme was relatively easy to implement. As a first approximation for a small solar declination angle (δ) the ring shadow covers a latitude band from about $\sin^{-1}[(r_{\min}/r_{\mathrm{earth}}) \sin \delta] - \delta$ to $\sin^{-1}[(r_{\max}/r_{\mathrm{earth}}) \sin \delta] - \delta$. Figure 2 shows the annual hemispheric migration of this ring shadow, as well as the latitudinal extent of the shadow at any particular date. The maximum extent of the shadow occurs at the solstices and covers $\sim 13°$ degrees of latitude. On 21 December, the southern limit of the shadow occurs at 14.1°N and the northern limit occurs at 26.8°N. At the equinoxes, there is no shadow. The net annual reduction in globally averaged insolation due to this specific ring geometry and opacity is 17.6 W/m^2 (324.2 W/m^2 for the ring case versus 341.8 W/m^2 for the control).

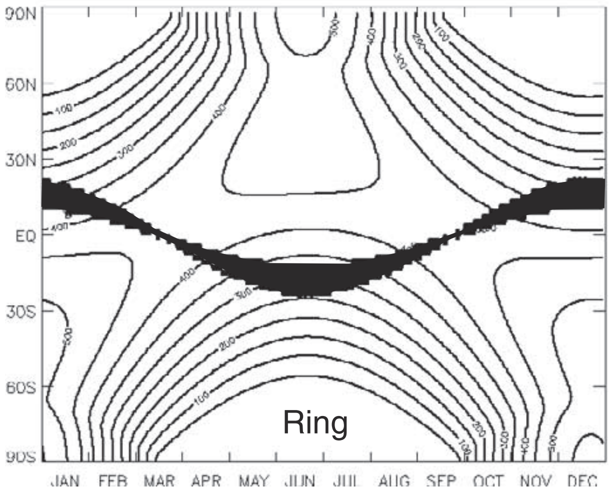

Figure 2. Solar insolation incident on a unit horizontal surface at the top of the atmosphere, modified by an equatorial debris ring in orbit. Area in black shows the extent of the ring shadow. Units in W/m^2.

2. Global Climate Model

[16] The climate model used in this study is GENESIS v.2 [*Thompson and Pollard*, 1997], an extensively modified version of the National Center for Atmospheric Research (NCAR) Community Climate Model (CCM1). This model (and an earlier version) has been widely used in a variety of modern and paleoclimate studies. The standard version of the model consists of an atmospheric general circulation model (AGCM) coupled to a land surface model (LSX), which consists of multilayer models of vegetation, soil, snow, and land ice. Sea surface temperatures are computed using a 50-m slab ocean model coupled to the AGCM, which crudely captures the seasonal heat capacity of the surface mixed layer. A thermodynamic sea ice model predicts the extent and thickness of sea ice. Poleward oceanic heat transport is treated as a horizontal diffusion down the gradient of the mixed-layer temperature with the diffusion coefficient depending strongly on the zonal fraction of land versus water and on the latitude itself [*Pollard and Thompson*, 1997]. This ocean heat flux parameterization is based only on observed estimates and is not a "flux correction" method, which allows the model to be used for different paleoclimatic applications [*Pollard and Thompson*, 1997].

[17] Atmospheric variables including mass, heat, and momentum are calculated as a set of spherical harmonics that are truncated at wave number 31 (T31) that is equivalent to a gaussian grid of 3.75° latitude by 3.75° longitude. The surface model was run on an equivalent grid.

[18] The present-day performance of the model is comparable to that of other coarse-grid models with predicted sea surface temperatures. Reasonable values are predicted for monthly mean surface temperatures and the diurnal range of temperatures, energy fluxes in the atmosphere, jet stream maximum strengths, and the locations of precipitation maxima [*Pollard and Thompson*, 1997].

3. Climate Model Results

[19] In this section, we present the main results of the Earth ring simulation and compare its climatology to a control simulation run with present-day boundary conditions. The ring simulation was run for 16 years and did not achieve a full equilibrium state by this time. However, the rate of change of globally average surface temperature decreased to less than 0.1°C/yr by year 13 of the run. As we are comparing the gross features of this climatology to the control and the differences are so large (due to the extreme nature of the forcing), these comparisons are significant within the uncertainty of how much sunlight a debris ring would actually block. The results presented are the averages of the last 4 years of both simulations.

[20] The equatorial debris ring has a profound effect on climate because it reflects a significant fraction of tropical insolation back to space before it can interact with the atmosphere. All aspects of Earth's climate are affected by this seasonal loss of insolation including surface and atmospheric temperatures, equator-to-pole temperature gradients, atmospheric circulation patterns, and the hydrological cycle. We do not attempt a complete and comprehensive analysis of this ring climatology; rather we focus on the climatic highlights that have some likelihood of being preserved in the geologic record.

3.1. Surface Temperature

[21] The global, annually averaged surface temperature for the ring simulation is 5.4°C, which is 9.5°C colder than

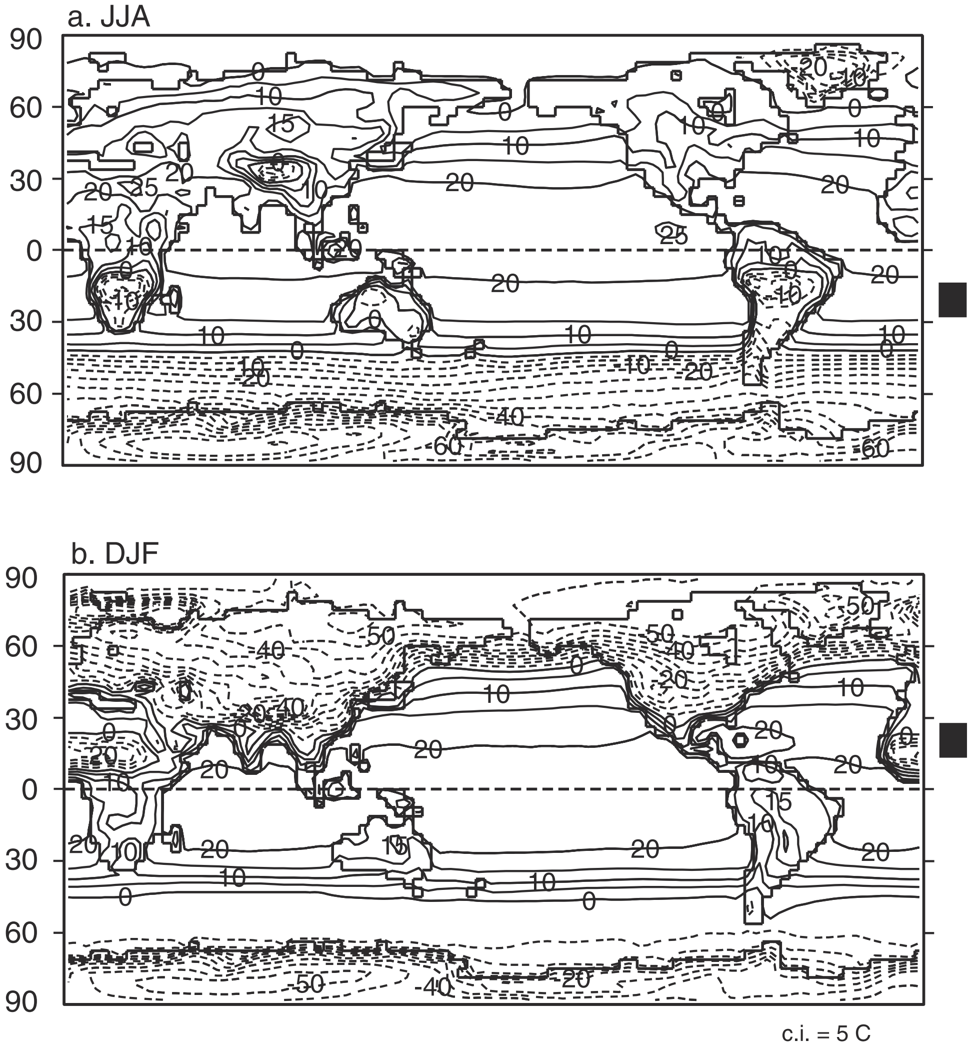

Figure 3. Model predicted surface temperature for the ring shadow simulation (5°C contour interval): (a) June-July August (JJA) and (b) December–January–February (DJF). Latitudinal ranges of the ring shadow at the solstices are shown as black boxes to the right.

the control (14.9°C). The ring shadow is primarily responsible for this cooling, although secondary positive feedbacks within the climate system act to amplify the global cooling. The surface temperature for both the summer and winter seasons (depending on the hemisphere), December, January, February (DJF) and June, July, August (JJA) are shown in Figure 3. In both seasons, the tropical sea surface temperatures reach a maximum of about 22°C. Tropical landmasses in both seasons average 10–15°C and only rise above 20°C in a few localities, and there is a marked winter cooling of subtropical landmasses that are under the ring shadow. The interiors of South Africa, Australia, and South America are substantially below freezing in JJA (−15 to −20°C), as is the interior of Saharan North Africa in DJF. The Northern Hemisphere continents are all below freezing in DJF (Figure 3a) with interior temperatures of −20°C and colder. Only the southernmost coastal areas have winter temperatures above freezing. Eurasia and North America experience cool summers where surface temperatures do not exceed 20°C. The high Tibetan Plateau has subfreezing JJA temperatures and is therefore frozen year-round. In the high latitudes, the 0°C isotherms are displaced equatorward relative to the control in both seasons: the Southern Hemisphere undergoes a larger displacement.

[22] Zonally averaged surface temperatures for DJF and JJA (Figure 4) show that the ring simulation is on average about 8°C colder than the control, and there are latitudinal bands where the temperature differences are much larger. Two of these bands at 15° to 20° north (DJF) and south (JJA) lie under the average positions of the seasonal ring shadows, and two more are at higher latitudes corresponding to the equatorward shift of the 0°C isotherm (and the sea ice margin). There is a very small sea ice related peak at 55 degrees N in JJA. The ring simulation has much shallower equator-to-pole surface temperature gradients in the summer hemispheres relative to the control (Figure 4). The meridional temperature gradient from the equator to about 40° latitude is decreased in the winter seasons. Temperature gradients poleward of this point increase and match those of the control simulation. In the subtropics, the local meridional temperature gradients are significantly steeper relative to the control on the equatorial margin of

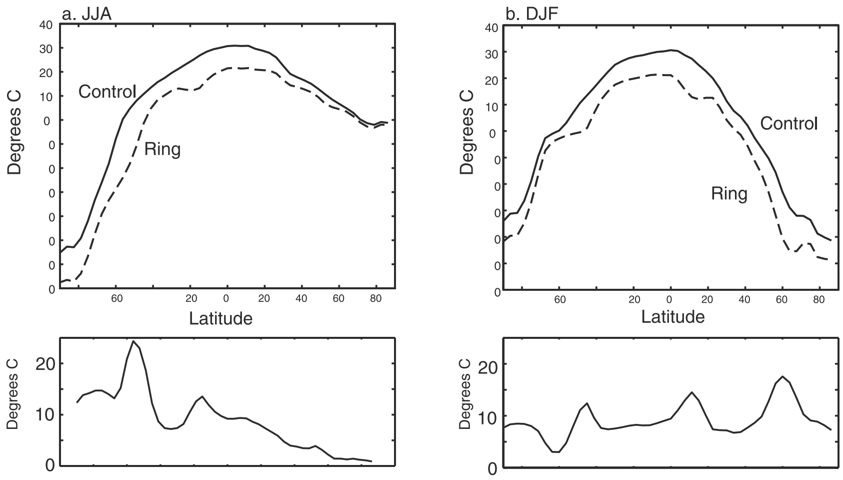

Figure 4. Zonally averaged surface temperature for two simulations. The solid line is the control experiment, and the dashed line is the ring shadow experiment: (a) JJA and (b) DJF. The absolute temperature differences for both seasons are plotted below.

the ring shadow while a relatively flat gradient occurs under the shadow itself (Figure 4).

[23] The spatial distribution of surface temperature differences between the control and the ring simulations is shown in Figure 5. In DJF, the largest differences occur in Saharan north Africa (up to 40°C), Alaska, and over the north Atlantic at 60°N. The interiors of other Northern Hemisphere landmasses are all colder by 10°C or more in the ring simulation. In the Southern Hemisphere, a zone of 10°C difference occurs at 45°S, while the interiors of south Africa, Australia, southern South America, and Antarctica are all 10°C colder than the control. In JJA, the largest surface temperature differences occur in Southern Hemisphere landmasses (up to 20 to 30°C) and in a zonal band at 50°S latitude. In the Northern Hemisphere summer, northern Africa, India, and the Tibetan Plateau are colder than the control by 10°C (Figure 5a). The interiors of Eurasia and North America are only 5°C cooler than the control in most places, and in eastern Siberia, the ring simulation is actually 5°C warmer than the control.

[24] In both seasons, the oceanic surface temperature differences under the ring shadows are not significantly greater than the surrounding ocean regions except in a few places. This is primarily due to the heat capacity of the ocean model mixed layer, which buffers temperature change at the surface. The model also has a diffusive ocean heat parameterization that advects heat into the shadow region rather quickly, and for this case, probably unrealistically. The surface air temperature differences (not shown), are larger than the surface temperature differences.

3.2. Atmospheric Pressure

[25] The patterns of semipermanent and seasonal highs and lows in the ring simulation are grossly similar to the control patterns but their locations are shifted in many cases, and their relative strengths are modified in a complex fashion. The most striking differences are the weakened high-latitude winter lows, the weakened winter subtropical highs, and the strengthened summer continental lows over the major monsoonal regions of the world (Figures 6 and 7). The differences in sea level pressure between the control and ring simulations (Figure 7) are difficult to interpret without discussing concurrently the positions and strengths of highs and lows in the ring simulation (Figure 6). In DJF, the Aleutian and Icelandic lows are present but are weakened with respect to their control counterparts (core pressures are higher by up to 18 and 8 mbar, respectively, Figures 6a and 7a). The Aleutian Low actually becomes two separate low-pressure centers with one located just east of Japan and the other, deeper low centered over the Alaskan panhandle (Figure 6a). At approximately the same latitude band, the high pressures in the interiors of Eurasia and North America are strengthened relative to the control by 2 to 6 mbar (Figure 7a). Winter subtropical high-pressure belts are weakened in the eastern Atlantic and in the eastern Pacific (by up to 8 mbar) in the ring simulation. In contrast, the subtropical continental highs present in the control over northern Africa and India are strengthened considerably in the ring simulation (by up to 10 mbar over the Sahara). The smaller high over Central America is also strengthened by about 2 mbar in the ring simulation. The stronger continental high-pressure zones all lie under the ring shadow. In the Southern Hemisphere, the summer thermal lows over the interiors of south Africa, Australia and South America are deepened by 2 to 4 mbar in the ring simulation (Figure 7a) strengthening these small monsoonal circulations. The prominent subpolar zonal low around Antarctica is weakened by 4 to 6 mbar.

[26] The JJA sea level pressure differences between the ring and control simulations are enhanced relative to DJF. Strong thermal lows are developed over all of the major Northern Hemisphere landmasses in the ring simulation (Figure 6b) which results in much stronger summer monsoonal circulations (discussed below). These surface lows are considerably deeper than their control simulation counterparts (pressures are lower by up to 8 mbar over northern Africa, 16 mbar over the Tibetan Plateau, and 10 mbar over SW North America) but are found in approximately the same locations. The Pacific High is strengthened considerably in the ring simulation and displaced slightly to the

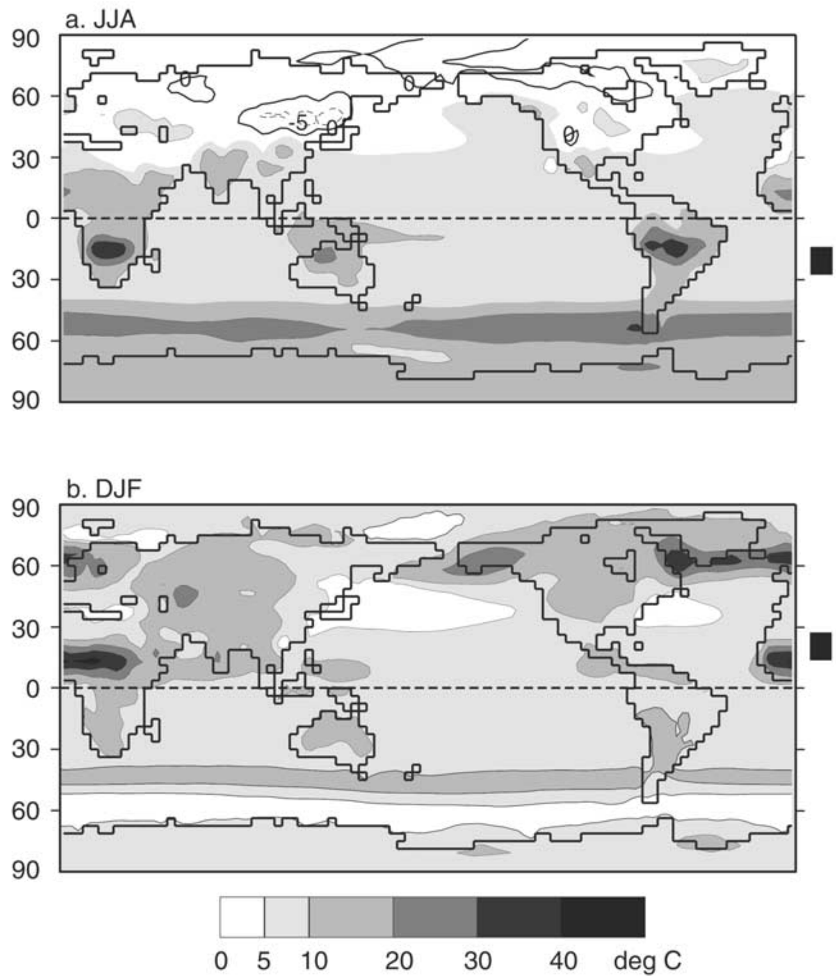

Figure 5. Average surface temperature differences (control minus ring shadow): (a) JJA and (b) DJF. Variable contour interval, see legend. Negative difference contours are dashed. Latitudinal ranges of the ring shadow at the solstices are shown as black boxes to the right.

north (Figures 6b and 7b). The Bermuda High is not greatly changed in strength or location, although sea level pressures are lower by 8 mbar in the Azores region. The tropical low-pressure zone is similar in both simulations.

[27] The winter (JJA) highs over the three Southern Hemisphere middle-latitude landmasses are strengthened, while the oceanic subtropical high-pressure zones are weakened by 2 to 4 mbar (Figures 6b and 7b). The circum-Antarctic low-pressure belt is weakened considerably relative to its control counterpart with pressure higher by up to 14 mbar (Figure 7b). The Antarctic high pressure is weakened by up to 8 mbar so that this high-latitude land-sea pressure contrast is reduced relative to the control simulation.

3.3. Surface Wind Patterns

[28] The large-scale surface wind patterns for DJF and JJA for the ring simulation (Figure 8) are not substantially different from those of the control (not shown), but there are important differences in some aspects of the circulation. In most cases, these are related to the differences in sea surface temperatures and in sea level pressure fields between the two simulations. In the tropics and the subtropics, the trade winds on either side of the equator are not significantly strengthened or weakened, but the Intertropical Convergence Zone (ITCZ) is shifted by a few degrees of latitude into the summer hemisphere.

[29] In JJA, stronger anticyclonic flow around the north Pacific High penetrates well into eastern Siberia and stronger northwesterly winds flow along the west coast of North America. A similarly strengthened pattern is seen over the North Atlantic with stronger winds flowing along the east coast of North America and the northwest coast of Africa (Figure 8a). In this simulation, the Atlantic trade winds do not penetrate into the interior of northern South America while in the control, they do. All of the Northern Hemisphere monsoon regions experience stronger southerly winds and enhanced convergence in JJA relative to the control. The areas most strongly affected are northern Africa, the SW Asia and the Indian subcontinent and SW North America. The low-level Somali Jet is considerably strengthened in the ring simulation, as is the low-level southern plains jet in North America. In the Southern Hemisphere winter, the axis of strong westerlies is shifted

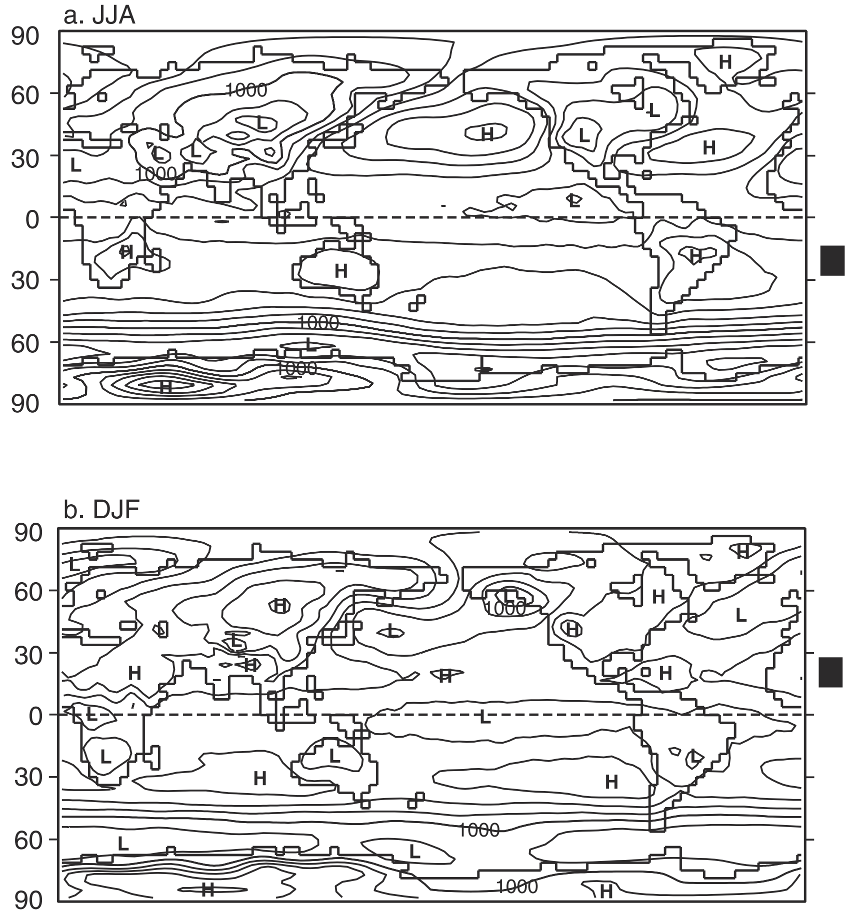

Figure 6. Model predicted sea level pressure (5 mbar contour interval) for the ring simulation: (a) JJA and (b) DJF. Positions of highs and lows marked with H and L, respectively. Latitudinal ranges of the ring shadow at the solstices are shown as black boxes to the right.

south from about 45°S (control) to about 60°S (ring). Cyclonic flows are better developed over the Southern Hemisphere continents (excluding Antarctica) in the ring simulation in response to higher surface pressures under the ring shadow.

[30] In DJF, the westerlies across both the Pacific and the Atlantic Oceans are significantly weaker than in the control. The strong anticyclonic circulation in the North Atlantic control simulation is absent in the ring simulation, and the strong anticyclone over Greenland pushes further to the south (Figure 8b). As in the Southern Hemisphere winter, the winter trade winds at the poleward side of the ring shadow weaken as the trade wind belt shifts south. In the summer hemisphere, summer monsoonal winds are strengthened over south Africa, northern Australia and both east and west central South America. The position and strength of the Southern Hemisphere summer westerlies are not significantly changed relative to the control.

3.4. Longitudinally Averaged Zonal Winds

[31] A latitude-pressure (height) cross section of longitudinally averaged zonal wind is shown in Figure 9 for January and July of both simulations. Important differences occur in both the summer and winter hemispheres including the strength and locations of the tropospheric westerly jets and of the subtropical easterlies at the tropopause up into the stratosphere.

[32] Two prominent maxima in zonal wind speeds occur in the Southern Hemisphere winter of the ring simulation (July, Figure 9a). One is located at approximately 30°S and occurs as a distinct jet while the other is located at 60°S and occurs as a downward extension of strong westerlies from the stratosphere into the lower troposphere. The core speeds in both the winter and the summer jets are reduced in the ring simulation relative to the control. The summer jet undergoes a larger relative decrease with core wind speeds just above 5 m/s compared to 15 m/s in the control.

[33] The most significant new pattern found in the ring simulation is a strong easterly jet that forms in July in the Northern Hemisphere subtropics. This jet is centered at the tropopause and extends up into the stratosphere (Figure 9a). The stronger subtropical easterlies in the ring simulation extend down through the troposphere to the surface resulting in two distinct features. The easterly belt is widened in the middle troposphere and at the surface, and the surface to lower troposphere zonal winds are stronger than in the control.

[34] The January summer and winter middle latitude westerly jets (Figure 9b) are reduced in strength relative to the control, but both occupy roughly the same positions

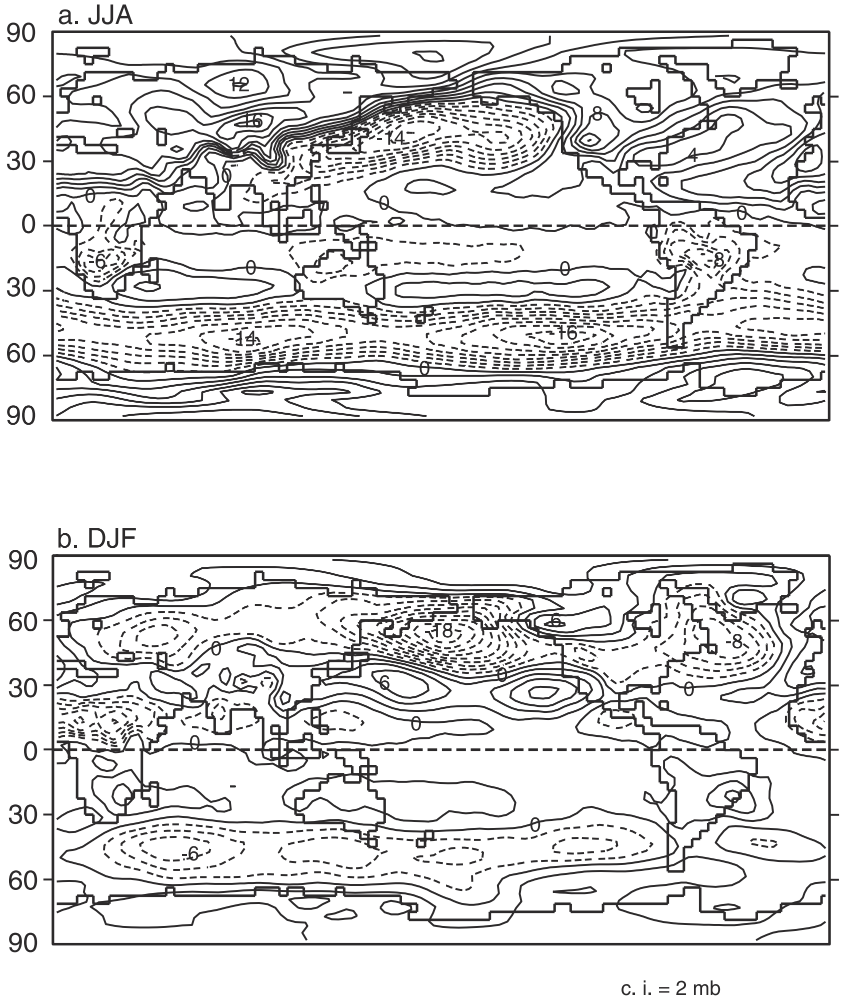

Figure 7. Average sea level pressure differences (control minus ring shadow): (a) JJA and (b) DJF. Contour interval is 2 mbar. Negative differences (dashed lines) indicate higher pressure in the ring simulation and positive differences (solid lines) indicate lower pressure in the ring simulation relative to the control simulation.

as their control counterparts. There is no second, poleward zonal wind speed maximum in the Northern Hemisphere in January. In the Southern Hemisphere, subtropical easterlies are stronger in the ring simulation at the tropopause, but no distinct easterly jet is developed as it is for the Northern Hemisphere summer. The surface to lower troposphere easterlies south of the equator are stronger than in the control.

4. Hydrological Cycle

[35] All of the changes discussed so far in temperature fields and atmospheric circulation patterns have a profound effect on the global hydrologic cycle. In this section, we examine changes in precipitation rates and patterns, evaporation rates, and snow cover and sea ice changes.

4.1. Precipitation

[36] All of the major features in modern global precipitation patterns are present in the ring simulation (Figure 10) including the Intertropical Convergence Zone (ITCZ), the secondary middle latitude precipitation maxima, monsoons, and dry polar winters. However, there are substantial differences with the control both in amounts of precipitation and in some of the spatial patterns of precipitation. Overall, the ring simulation is considerably drier. The global mean annual precipitation rate is 71% of the control value, although it should be noted that the control simulation precipitation rates are higher than observed [*Thompson and Pollard*, 1997]. Zonally averaged precipitation rates for the control and ring simulations are shown in Figure 11 for JJA and DJF. The largest zonal differences occur at the equator and the smallest occur at the poles. A prominent, secondary precipitation maximum on the poleward side of the ring shadow is another unique feature of the ring shadow simulation. While this feature is evident in the winter hemisphere of the zonally averaged precipitation plot (Figure 11), the maxima only occur over the ocean (Figure 10). Similar secondary precipitation maxima occur in the control simulation (not shown), but they are not as pronounced and are found more in the middle latitude regions.

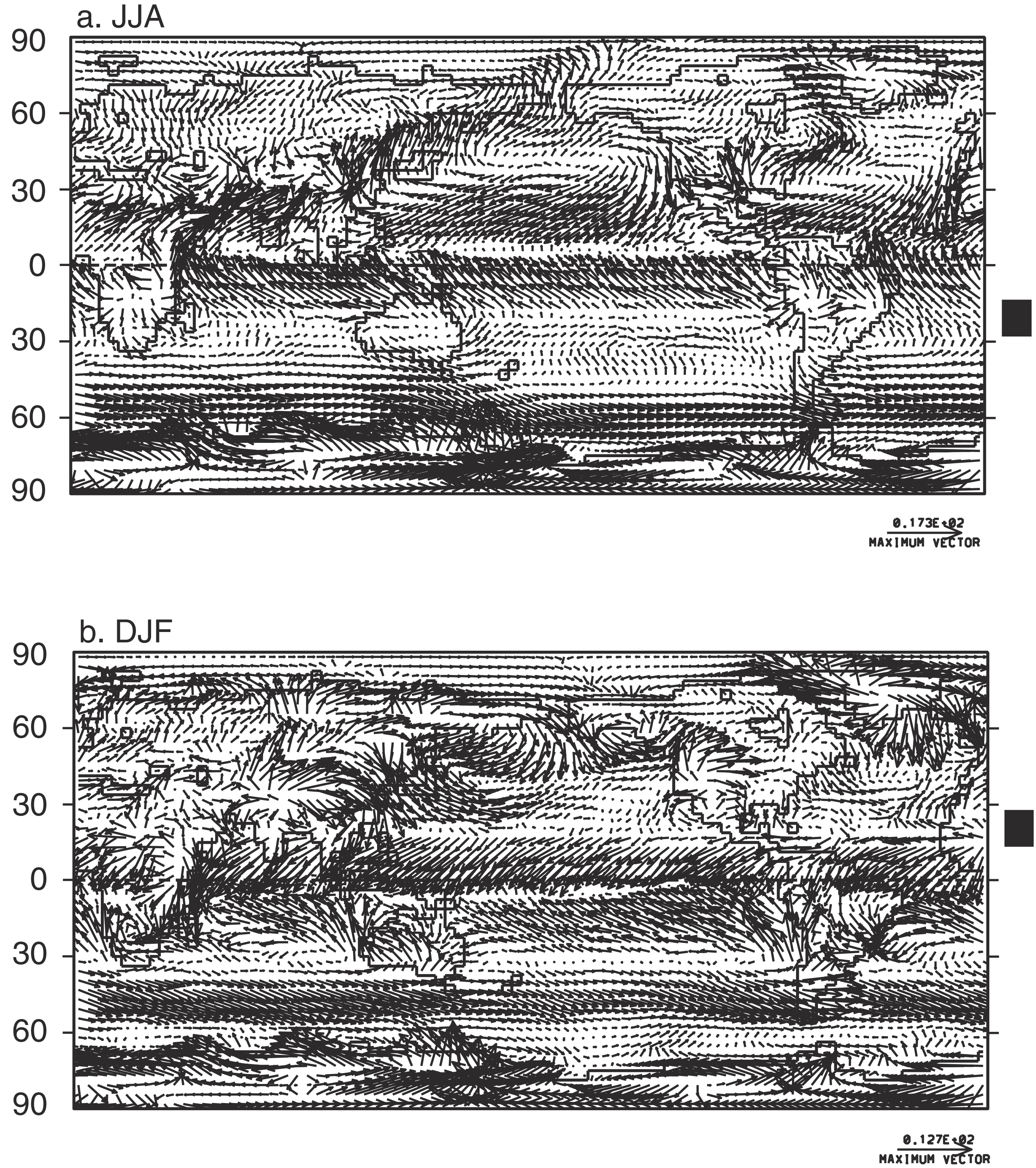

Figure 8. Model predicted surface winds for the ring simulation: (a) JJA and (b) DJF. Maximum wind vector is given for each season in m/s. Latitudinal ranges of the ring shadow at the solstices are shown as black boxes to the right.

[37] Precipitation difference plots (Figure 12) show that over most parts of the globe, the control simulation is considerably wetter than the ring simulation. The areas of greatest difference are in the tropics in general and within the ITCZ specifically where differences can be as large as 12 to 18 mm/d. Precipitation differences are smallest over high-latitude regions and midlatitude land areas in winter. Despite an overall drier global climate in the ring simulation, subtropical monsoon regions are much wetter than in the control. The largest area of enhanced summer precipitation extends from western North Africa across the Arabian Peninsula into the northern part of the Indian subcontinent

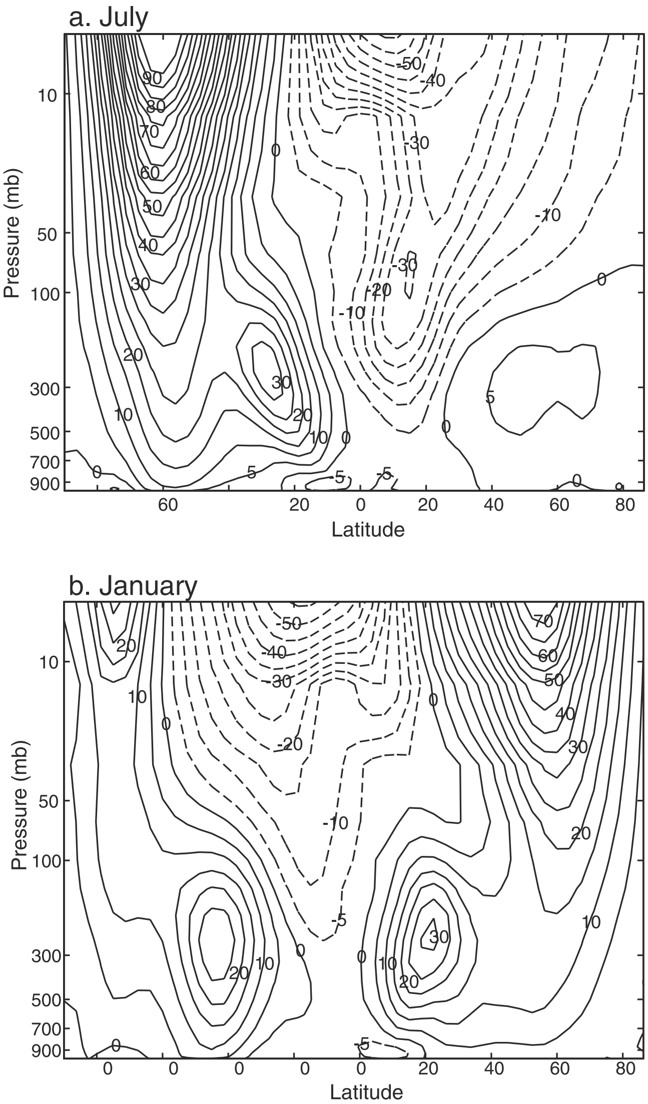

Figure 9. Model predicted meridional cross section of longitudinally averaged zonal winds (5 m/s contour interval) for the ring simulation: (a) July and (b) January.

(Figure 12a). At the core of this enhanced monsoon region in the ring simulation, precipitation rates are up to 9 mm/d higher than the control (e.g., Saharan North Africa). Southwestern North America and most of northern Mexico also show large positive summer precipitation anomalies relative to the control. Except for one location on the equator, southeast Asia shows a precipitation decrease in the ring simulation in contrast to the other monsoon regions. Areas of nonmonsoonal summer precipitation increases include northern China and northeastern North America (Figure 12a). In the Southern Hemisphere, enhanced summer monsoons occur over south Africa, northern Australia and south-central South America. The maximum difference with the control is just over 3 mm/d in Australia (Figure 12b). At higher latitudes, a marked decrease in precipitation rates (3 mm/d) occurs in a belt over the oceans centered at 45°S (Figure 11b, 12b).

[38] Precipitation differences in the winter season of both hemispheres are also significant. In all of the subtropical monsoon regions, negative precipitation anomalies (i.e. wetter in the ring simulation) persist from summer (Figure 12) suggesting a positive feedback from soil moisture anomalies. Winter precipitation values show a decrease of 1 to 4 mm/d at 40°N latitude in the ring simulation. The largest positive anomalies occur in the eastern Pacific and northwestern North America, the North Atlantic and Europe into central Asia (Figure 12b). In the Southern Hemisphere, the largest positive anomalies (3 to 4 mm/d) occur in a belt over the southern Ocean centered at 45°S (Figures 11a and 12a).

4.2. Evaporation

[39] In both JJA and DJF, zonally averaged evaporation rates are consistently lower in the ring simulation by 0.25 to 3 mm/d (Figure 13). In this simulation, evaporation rates are highest just poleward of the equator in the winter hemisphere where surface winds are higher. Zonal rates fall rapidly just poleward of these maxima between 15° and 25° of latitude (north or south depending on the season). The largest differences with the control occur in the tropics (roughly between 20°S and 20°N) and there are three distinct difference peaks evident in both seasons (Figure 13). One peak occurs between 15° and 20° of latitude in the winter hemisphere, corresponding with the seasonal ring shadow. The second peak occurs in the summer hemisphere subtropics (about 15° latitude) where surface winds are weaker in the ring simulation. The third peak occurs in both seasons between 45° and 50°S where evaporation rates are considerably lower in the ring simulation because of a significant poleward advance of sea ice (section 4.3). Evaporation rate differences are lower at higher latitudes elsewhere, and are minimized between 20° and 30°N where summer monsoons are stronger in the ring simulation.

4.3. Sea Ice and Snow Cover

[40] The predicted amounts of sea ice and snow cover for the ring simulation show dramatic increases relative to the control simulation and act as a powerful positive feedback to the global cooling. Both sea ice extent and snow cover thickness are combined into single plots for JJA and DJF (Figure 14) as the sea ice margin (not shown) closely corresponds to the snow cover limit over the oceans.

[41] Sea ice in the Southern Hemisphere winter (JJA, Figure 14a) extends from the Antarctic coast to about 35°S, a considerable equatorward expansion relative to the control. The Drake Passage is effectively closed to surface ocean circulation and the sea ice limit also reaches southernmost Australia and New Zealand. Significant amounts of snow cover (>10 cm thickness) occur over South Africa, Australia and South America where the snow cover extends to 10°S latitude in the Amazon Basin. The areas of thickest snow cover occur over Antarctica and Patagonia. In the Northern Hemisphere summer, the sea ice margin lies at about 55°N in both the Atlantic and Pacific Oceans. Summer snow cover persists across northern North America, eastern Siberia and northwest Europe as well as over the Tibetan Plateau.

[42] In the opposite season, DJF (Figure 14b), the Southern Hemisphere sea ice margin lies at 40°S, still closing the Drake Passage. Summer snows persist in Patagonia, the central Andes, New Zealand, and Tasmania and in south-

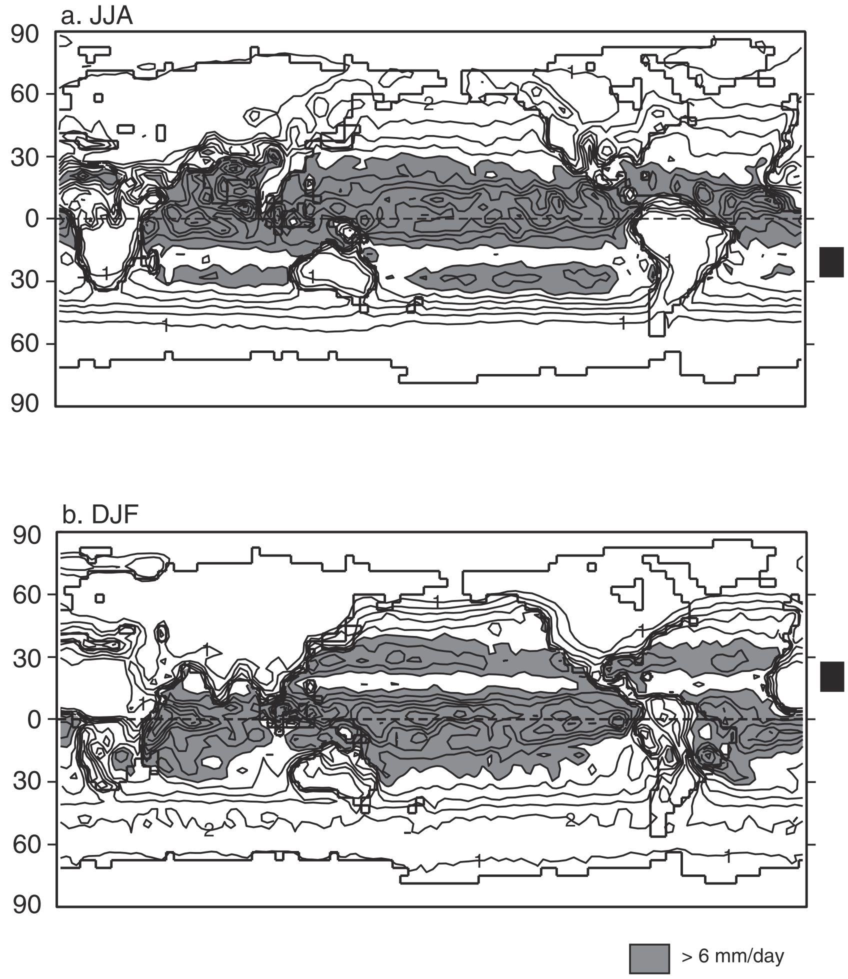

Figure 10. Model predicted precipitation rates (contour interval of 1 mm/d) for the ring simulation: (a) JJA and (b) DJF. Areas of precipitation greater than 6 mm/d are shaded.

ernmost South Africa. The Northern Hemisphere sea ice front migrates to 50°N and virtually all of the major landmasses are snow covered. Snow cover reaches to within 10°N of the equator in Saharan north Africa, southern India, southeast Asia, and covers almost all of Mexico. Areas of significant snow depths include the North American cordillera, central to eastern North America, Greenland, the Tibetan Plateau, and eastern Siberia. Higher snow depths also occur across Europe.

5. Discussion

[43] The main goal of this study is to describe the possible long-term effects of large, oblique planetary impact events that are capable of inserting significant quantities of material into orbit. While no definitive case for such an impact has been made from the geologic record, calculated probabilities suggest that over the long span of Earth history several such events must have occurred [e.g., *Schultz and Gault*, 1990]. By using an atmospheric GCM, we have determined the possible climatic effects of a geologically temporary, equatorial debris ring. In all likelihood, Earth would not have experienced the full extent of the climatic effects reported here if a debris ring had formed, because it is unlikely that the ring would be fully opaque. However, these results can guide interpretations of the geologic record where the effects would be similar but not as extreme as depicted here.

5.1. Ring Shadow Climatology

[44] The effects of a fully opaque debris ring in orbit around the equator are profound and wide-ranging. Almost all aspects of the simulated climate system are affected by the loss of insolation in the subtropics of the winter hemisphere. The immediate effect of the ring shadow is a dramatic cooling of the tropical oceans and subtropical landmasses. Directly under the shadow, the ocean does not cool as much as the land due to its greater heat capacity and its ability to advect heat laterally. This lateral advection of heat from the tropics into the subtropical ring shadow region is partly responsible for the tropical cooling and there is much less heat available for export to the middle and high latitudes. At the higher latitudes, snow cover extent increases and the sea ice margins expand equatorward, acting as a powerful positive feedback to the global cooling. Snow cover persists year-round in several high-latitude and high-altitude locations including the Tibetan Plateau, Patagonia, northern Canada, and the northern fringe of Eurasia (Figure 14).

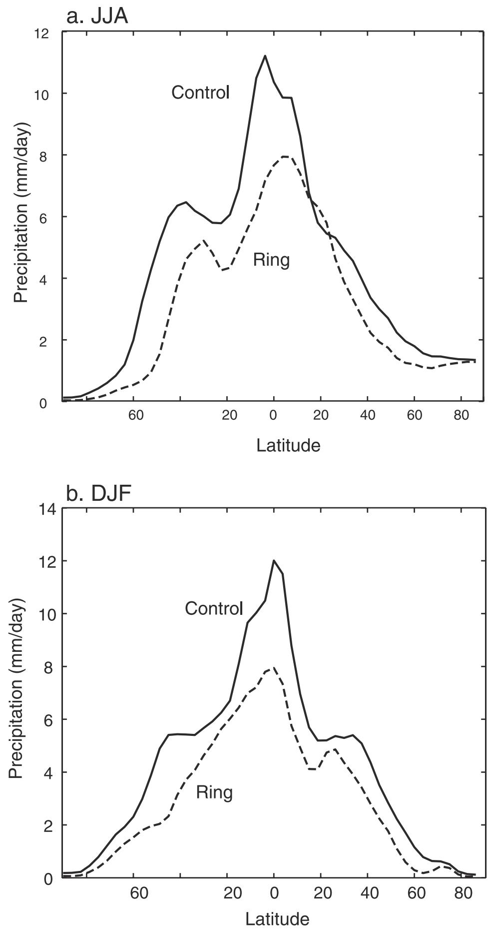

Figure 11. Zonally averaged precipitation rates for two simulations. The solid line is the control experiment, and the dashed line is the ring shadow experiment: (a) JJA and (b) DJF.

[45] As discussed earlier, this simulation was close to, but not fully, in equilibrium after 16 years (the change in global temperature during the last 4 years of the simulation was less than 0.1°C). We expect that the sea ice margins would continue their equatorward migration and enhance the global cooling, although it is unlikely that a "snowball Earth" scenario would result with the present-day solar constant and atmospheric CO_2 concentrations.

[46] The cooler surface temperatures of the ring shadow simulation significantly reduce evaporation rates, especially in the tropics. The strength of the Hadley cell circulation is weakened because the cooler tropical sea surface temperatures promote less deep convection and a lower atmospheric water vapor content. The weakened Hadley circulation reduces the strength of oceanic subtropical highs in the winter hemisphere (Figure 7). Over winter hemisphere subtropical landmasses, however, stronger high-pressure cells are the result of the intense cooling under the ring shadow.

[47] One of the most surprising results of the ring shadow simulation is the tremendous strengthening of summer monsoon winds and rainfall amounts. The area most affected is northern Africa (Figures 10 and 12), but the other major monsoon regions of the world are also enhanced. This result is not intuitive because the summer hemisphere land surface temperatures are markedly cooler than in the control. As the land-sea thermal contrast is the major driving force for a monsoon circulation, the cooler land surface temperatures alone should promote a weaker monsoon. However, in the ring simulation, the degree of tropical and subtropical ocean cooling is actually larger than in the interiors of the large continents including Asia, northern Africa/Arabia, and North America (Figure 4). This occurs because the ring shadow in the winter hemisphere draws a massive export of surface ocean heat across the equator from the summer hemisphere into the winter hemisphere. By this process, the ring shadow actually enhances the land-sea thermal contrast in the major monsoon regions of the world. The resulting summer monsoon winds are stronger (e.g., the low-level Kenyan jet, Figure 8a) and transport more moisture into the interiors of Asia, Africa, and North America. Land surface temperatures are still warm enough to promote cumulus convection, and the additional latent heat release from the extra moisture convergence helps to strengthen all of these monsoonal flows. The surface lows in the summer monsoon regions are considerably deeper, and have wider spatial extents in the ring simulation (Figures 6 and 7). The same process works in the Southern Hemisphere summer (DJF) to strengthen these monsoons (Australian, northern South America) relative to the control, but because the landmasses are smaller, the monsoons are still relatively small.

[48] The presence of stronger monsoon circulations in the ring simulation, especially over Asia and northern Africa, has significant effects on other parts of the climate system. An intense tropical easterly jet forms in the summer near the tropopause above central Asia and accelerates to the east over northern Africa. This jet forms on the equatorward side of a strong, upper level high over Tibet (paired with the deep surface low) where the contrast in temperatures between this region and the air above the ocean to the south produces a strong north-south pressure gradient and easterly winds. Regions affected by the stronger summer monsoons are considerably wetter in the ring shadow simulation and the precipitation anomalies persist into winter (Figure 12). This is especially evident over north Africa, Arabia, and SW North America where the winter cooling is largest (ring shadow). The cold temperatures severely curtail evaporation rates and promote the buildup of snow cover in the subtropics (Figure 14).

[49] Tropospheric winds are weakened in the ring simulation, especially the middle-latitude westerly jets (Figure 9). The weakened winds are a direct consequence of the ring shadow blockage of insolation in the tropics, and a shallower equator to pole temperature gradient (Figure 4). In the winter hemisphere, there is a split in the upper level westerly jet stream, especially in the Southern Hemisphere (Figure 9). The second, subtropical jet forms near the strong temperature contrast on the poleward side of the ring shadow.

[50] Winter high-latitude low-pressure cells including the Aleutian low, the Icelandic low, and the circum-Antarctic subpolar low are considerably weakened (Figures 6 and 7). The weakened winter lows imply reduced baroclinic instability in the middle latitudes and fewer and/or

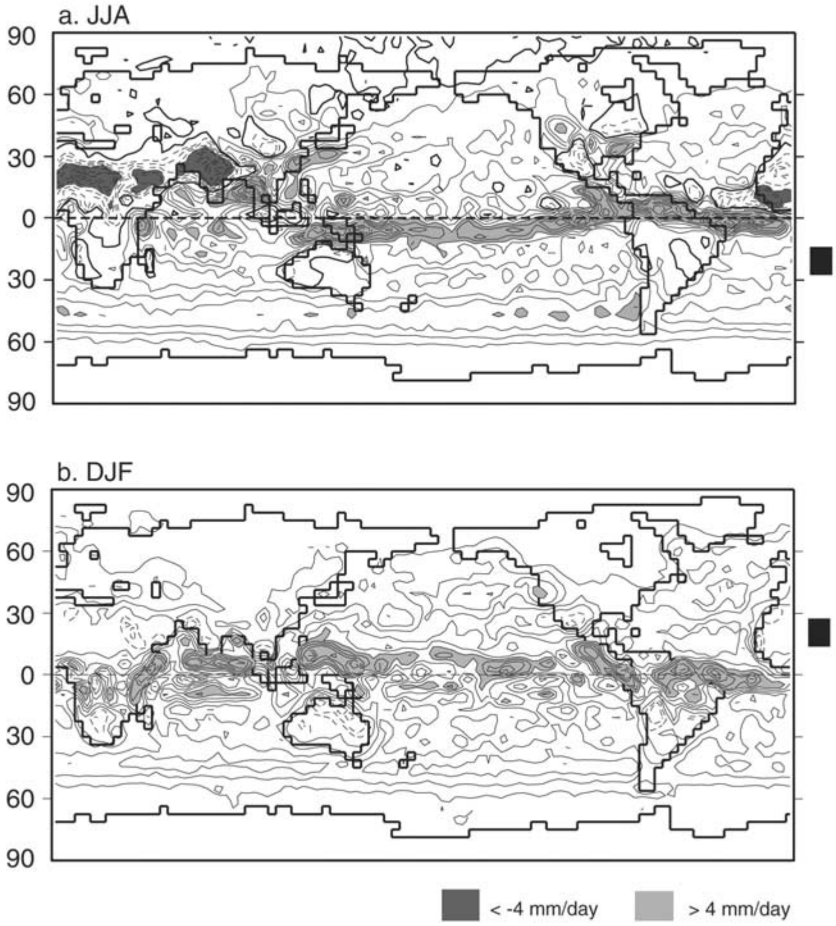

Figure 12. Average precipitation rate differences (control minus ring shadow): (a) JJA and (b) DJF. Contour interval of 1 mm/d; negative differences (wetter areas in the ring simulation relative to the control) are dashed lines. Areas of difference greater than 4 mm/d are shaded as shown in legend. Zero contour line is the heavier black line. Latitudinal ranges of the ring shadow at the solstices are shown as black boxes to the right.

weaker winter storms. This appears to be the product of a reduced equator-to-pole temperature difference, and weakened subtropical highs in the winter hemisphere that weaken atmospheric flow in the middle latitudes. In addition, the winter sea ice margins are displaced equatorward and this moves the polar front equatorward over the oceans. In the northern summer, the Pacific High is considerably strengthened and is moved poleward in response to the enhanced summer monsoon over North America [cf. *Rodwell and Hoskins*, 2001]. Stronger southeasterly winds around this strengthened high are responsible for the warmer temperatures in eastern Siberia in the ring simulation (Figure 5) and help maintain the stronger summer monsoon over southeastern Asia.

5.2. Predicted Climatic Effects of a Ring Shadow in the Geologic Record

[51] If the Earth ever did have a geologically temporary, orbiting debris ring how would we know? Evidence from the sedimentary record (e.g., iridium anomalies [*Alvarez et al.*, 1980]) correlated with an impact structure is one way to tell if an impact has occurred, and estimates can even be made about the size of the impacting body. This information by itself, however, is not enough to determine if the impact occurred at a sufficiently low angle and with enough energy to insert material into orbit. On the basis of the climatology of the ring shadow simulation, we can make some essential predictions about what the climate preserved in the geologic record should look like during such an event. Such an analysis is complicated by two factors. First, a debris ring would in all likelihood not be fully opaque and the predictions made here would represent an extreme end-member climate. Second, the transient nature of such a climate perturbation would restrict its stratigraphic record and make global correlations difficult, especially in pre-Quaternary rocks. However, correlation of climate records from the sedimentary interval just above a global Iridium anomaly would help facilitate such an analysis.

[52] The primary signature of an orbital equatorial debris ring would be a dramatic cooling that persisted over a much longer interval than the immediate effects of a large impact (i.e., the time it would take for a stratospheric dust cloud to dissipate). The cooling would be

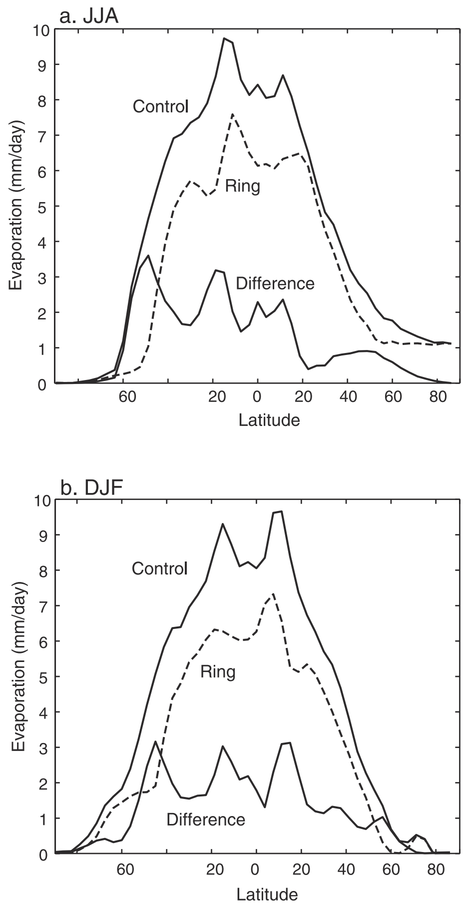

Figure 13. Zonally averaged evaporation rates for the control (solid line) and ring (dashed line) simulations: (a) JJA and (b) DJF. The absolute differences (mm/d) between the two are plotted also (heavy black line).

global, but enhanced in winter. The subtropics should see a larger cooling than surrounding regions, and the cryosphere would expand equatorward. The globe as a whole would be drier; especially in the tropics and so one might look for a shift in vegetation to drier types. The exception to the drier trend is the enhanced summer monsoons, which would increase precipitation in many areas. The magnitude of this effect would depend as much on the continental geometry of the time period (i.e., larger continents promote stronger monsoons) as the opacity of the orbiting debris ring.

[53] The reduced tropospheric wind speeds, especially in the cores of the westerly jets might be reflected in the geologic record as reduced atmospheric dust transport and smaller eolian grain sizes in ocean sediments [cf. *Rea et al.*, 1985]. The severely weakened high-latitude winter low-pressure cells and fewer/weaker storms would be difficult to discern in the geologic record apart from the resulting lower precipitation rates.

5.3. Assessment of the Geological Record

[54] The number of recognized large impacts in the geologic record has increased every year since Alvarez et al.'s seminal paper in 1980, but many more will undoubtedly be found in the future. Of the currently known impact events, there are a few potential candidates for an oblique, high-energy event that might have been capable of inserting material into orbit. In this section we assess the geologic record of climate following a late Eocene impact, the Cretaceous-Tertiary boundary event, and farther back in time during the Neoproterozoic. We suggest that of these events, the late Eocene is the most likely to have produced an orbiting debris ring and that the K-T boundary event did not. We also suggest that the Neoproterozoic "snowball Earth" episodes [*Hoffman et al.*, 1998] could have been started by a large, oblique impact and attendant debris ring.

[55] The late Eocene impact event was initially recognized on the basis of a meteoritic iridium anomaly, which is overlain by a microtektite layer [*Ganapathy*, 1982]. Two very closely spaced (stratigraphically) tektite strewn fields representing impact ejecta are now recognized at this time interval (35.5 Ma), the North American strewn field and the Pacific strewn field. Of the two, the Pacific strewn field is much larger spanning a wide circum-equatorial swath around the globe and it is now recognized at higher latitudes [*Vonhof and Smit*, 1999]. The 100 km diameter Popigai crater in Siberia is a possible source crater for the Pacific strewn field [*Vonhof and Smit*, 1999] and the North American strewn field has been linked to the Chesapeake Bay impact structure [*Koeberl et al.*, 1996]. *Wei* [1995] suggested that the two major strewn fields were, in fact, the same event, but no other author has made this claim. Whether these tektite strewn fields represent one or two events, the (near) global distribution of impact ejecta indicates that a large amount of material was accelerated to at least a suborbital trajectory and some fraction of this may have been inserted into orbit.

[56] The climatic record from the sedimentary interval immediately above the iridium/microtektite interval has been studied at two widely separated localities, the Massignano section in central Italy and at the Maud Rise in the Southern Ocean (Ocean Drilling Project site 689). Both sections show a cooling event of about 2°C with an estimated duration of 100 kyr [*Vonhof et al.*, 2000]. At the Maud Rise, $\delta^{13}C$ data show a surface water productivity increase that is attributed to the cooling. The authors of this study point out that 100 kyr is too long a cooling to be explained by an impact event alone and suggest a feedback mechanism involving more snow and ice cover maintained the cooler temperatures. We suggest that an orbiting debris ring casting its shadow in the subtropics could have sustained this extended postimpact cooling. The estimated lifetime of such a ring is on the order of 100 kyr to $\sim$1 Myr [*Schultz and Gault*, 1990], similar to the duration of this climatic event. The magnitude of the cooling is much smaller than in the ring shadow simulation, which suggests that if a debris ring was responsible, it was probably not opaque.

[57] *O'Keefe* [1980a] originally suggested that an orbiting tektite ring (of lunar origin) could explain a major climatic change at the Eocene-Oligocene boundary. Indeed there are many aspects of climate change from the Eocene to the Oligocene that are grossly similar to the ring shadow predictions, and these include a global cooling [e.g., *Wolfe*, 1978; *Zachos et al.*, 1994] a buildup of ice on

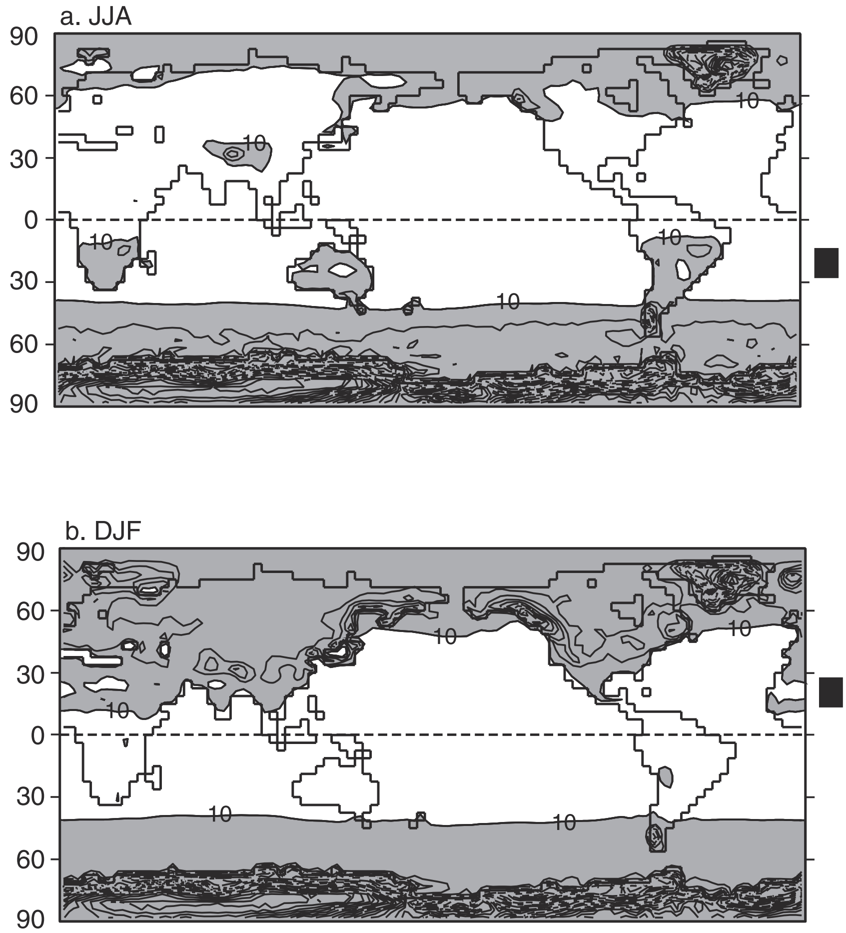

Figure 14. Model predicted snow cover and sea ice distribution for the ring simulation: (a) JJA and (b) DJF. Snow thickness contour interval is 10 cm. Sea ice margin is equivalent to the 10 cm contour over ocean areas.

Antarctica [e.g., *Zachos et al.*, 1992], a general trend toward drier vegetation types [e.g., *Fredricksen*, 1988; *Oboh et al.*, 1996], and at the boundary itself, a major extinction of marine invertebrates [*Raup and Sepkoski*, 1986]. *Ivany et al.* [2000] suggest that winters in the Gulf of Mexico became about 4°C colder with no apparent change in mean annual temperatures across the Eocene-Oligocene boundary. However, a closer examination of these changes at the boundary shows that they are unlikely to have been caused by an orbiting ring. A major problem is that the boundary occurs about 1.8 Myr after the impact events (33.7 Ma versus 35.5 Ma) so it becomes difficult to attribute cause (impact) and effect (boundary) with such a long lag. The cooling from the Eocene to the Oligocene actually takes place over several million years, and there is no discernable cooling at the boundary in low-latitude oceans [*Zachos et al.*, 1994; *Ivany et al.*, 2000]. *Wolfe* [1978] described the cooling from the Eocene to the Oligocene on the basis of vegetation changes, primarily in North America, which O'Keefe attributed to a ring. These vegetation changes occurred over millions of years, however, and are more consistent with a long-term climate change than a single abrupt event. We argue that a debris ring did possibly form during the late Eocene via an impact mechanism and did affect climate in a transient way, but it occurred before the Eocene-Oligocene boundary changes.

[58] The Cretaceous-Tertiary boundary impact was much larger than the late Eocene impact(s) and had a much larger immediate effect on Earth's environment, both in terms of extinctions [*Raup and Sepkoski*, 1986] and atmospheric perturbations [e.g., *Prinn and Fegley*, 1987; *Sigurdsson et al.*, 1992]. Once the immediate effects of the impact dissipated, there were no observed longer-term effects on the climate system. *Brinkhaus et al.* [1998] report no changes in sea surface temperatures above the impact horizon, and *Mukhopadhyay et al.* [2001] report lower deep-ocean carbonate sedimentation rates during the ~10 kyr of the K-T boundary clay deposition and then a return to preimpact values. The K-T boundary event probably did not generate a planetary debris ring, reinforcing the idea that the geometry of an impact is more important that the size of the impacting body in ring formation.

[59] One of the more interesting climatic episodes in Earth history occurred during the Neoproterozoic when the planet may have undergone a global glaciation or snowball Earth [*Hoffman et al.*, 1998; *Kirschvink*, 1992]. Part of the evidence for a snowball Earth is enigmatic low-latitude glacial deposits that *Crowell* [1983] suggested could be the

result of an equatorial ice ring. Assuming that the Earth had some degree of axial tilt from the ecliptic, a ring will only cast a shadow in the winter hemisphere subtropics and these regions will receive full summer insolation amounts. On the basis of the ring shadow simulation, the tropics and subtropics are still warm enough in summer to prohibit the formation of low-latitude, sea level glaciers. (However, high-elevation areas like Tibet are snow covered year-round.) Therefore an equatorial ring would not allow glaciers to grow in the tropics to the exclusion of higher-latitude regions. We do note, however, that with an opaque ring, the cooling of the tropics allows for an equatorward expansion of snow and ice cover and a positive feedback on the climate system. Given a reduction in solar insolation during the Neoproterozoic (about 5 to 6% lower than today [*Endal*, 1981]) and a sufficiently opaque debris ring, it is possible that a large, oblique impact could act as the trigger sending the Earth into a snowball Earth state. Once the Earth was in a high-albedo frozen state, the ring shadow would become less important and the Earth could remain in a frozen state for millions of years after the ring dissipated. A 150 km diameter impact structure, Acraman, has been found in the Neoproterozoic of Australia [*Williams*, 1994] and is estimated to have occurred at about 590 Ma which roughly matches the timing of one of the later episode of possible global glaciation (Marinoan ~600 to 575 Ma). We are unaware of any earlier craters so it is difficult to fully evaluate this as a possible mechanism for generating all episodes of Neoproterozoic snowball Earth. There are other plausible explanations for the onset of a global glaciation (tectonic effects, rapid drawdown of atmospheric CO_2 [*Hoffman et al.*, 1998]).

6. Conclusions

[60] Theoretical and laboratory studies suggest that some large impact events are capable of inserting material into orbit depending on the energy and angle of impact. This material would quickly coalesce to form a temporary debris ring in orbit around the equator. The orbiting ring would cast its shadow on the winter hemisphere and could drastically alter the climate system during its lifetime depending on the amount of material and opacity of the ring. The results of our ring shadow simulation with an atmospheric GCM show what kinds of effects could result under such a scenario. As a first order sensitivity test, we chose to use a fully opaque ring, which blocked all insolation under its shadow.

[61] A tremendous cooling in the winter hemisphere subtropics results from the ring shadow, especially over landmasses. The ocean surface cools and rapidly advects heat in from the surrounding ocean due to strong temperature contrasts. This cools the entire tropical ocean, which affects the rest of the climate system. High-latitude regions cool dramatically because of the reduced poleward heat transport from the tropics, especially in the winter hemisphere. Snow cover and sea ice margins advance toward the equator acting as a powerful positive feedback, cooling the globe even more. The equator-to-pole temperature gradient becomes shallower, especially in summer, which weakens tropospheric winds. Westerly jets are weakened in their core wind speeds, and a second, subtropical jet develops in the winter hemisphere on the equatorward side of the ring shadow. High-latitude winter lows are considerably weakened due to an overall reduction in baroclinic instability and storminess.

[62] In the tropics, the strength of the Hadley cell is reduced and the ITCZ while still present does not have as much rainfall. The subtropical oceanic highs in the winter hemisphere are weakened and this also contributes to the lower tropospheric wind speeds. With the drastic cooling of the tropical and subtropical oceans, subtropical land-ocean temperature contrasts are enhanced and this helps generate much stronger summer monsoons. Areas that are deserts today as well as current monsoonal areas become considerably wetter, and a strong easterly jet forms at the tropopause over central Asia. Everywhere else, the globe is drier because of the cooler sea surface temperatures and reduced evaporation rates.

[63] On the basis of this simulation, we made a number of predictions about what the climate record in the geologic column would look like if the Earth had an orbiting debris ring. Three impact events were evaluated in terms of their long-term effects on climate and we suggest that the late Eocene event is the most likely to have produced at least a moderately opaque orbiting debris ring. The K-T boundary most likely did not experience an impact-generated debris ring even though it was larger than the late Eocene event(s). Although much more remains to be learned about the Neoproterozoic snowball Earth, we suggest that an opaque debris ring could have acted as the trigger to at least one episode of global glaciation through the powerful tropical cooling and attendant high-latitude feedbacks.

[64] **Acknowledgments.** We thank Karl Wegmann for help in processing the model results and David Gutzler for reviewing an early version of this manuscript. Comments from three anonymous reviewers helped to improve the text. Grants to P.J.F. from the Sandia-University Research Program and NSF (ATM 00-00545) supported this work. This work was funded in part by the Sandia National Laboratories LDRD program (project 10318) and was supported by the U.S. Department of Energy under Contract DE-AC04-94AL85000. Sandia is a multiprogram laboratory operated by Sandia Corporation, a Lockheed Martin Company, for the U.S. Department of Energy.

References

Alvarez, L. W., W. Alvarez, F. Asaro, and H. V. Michel, Extraterrestrial cause for the Cretaceous-Tertiary extinction, *Science*, *208*, 1095–1108, 1980.

Barlow, N. G., Constraints on early events in Martian history as derived from the cratering record, *J. Geophys. Res.*, *95*, 14,191–14,201, 1990.

Boslough, M. B. E., and D. A. Crawford, Shoemaker-Levy 9 and plume-forming collisions on Earth, *Ann. N. Y. Acad. Sci.*, *822*, 236–282, 1997.

Brahic, A., Systems of colliding bodies in a gravitational field: Numerical simulation of the standard model, *Astron. Astrophys.*, *54*, 895–907, 1977.

Brinkhaus, H., J. P. Bujak, J. Smit, G. J. M. Versteegh, and H. Vischer, Dinoflagellate-based sea surface temperature reconstructions across the Cretaceous-Tertiary boundary, *Palaeogeogr. Palaeoclimatol. Palaeoecol.*, *141*, 67–83, 1998.

Covey, C., S. J. Ghan, J. J. Walton, and P. R. Weissman, Global environmental effects of impact-generated aerosols: Results from a general circulation model, in *Global Catastrophes in Earth History: An Interdisciplinary Conference on Impacts, Volcanism, and Mass Mortality*, edited by V. L. Sharpton and P. D. Ward, *Spec. Pap. Geol. Soc. Am.*, *247*, 263–270, 1990.

Covey, C., S. L. Thompson, P. R. Weissman, and M. C. MacCracken, Global climatic effects of atmospheric dust from an asteroid or comet impact on Earth, *Global Planet. Change*, *9*, 263–273, 1994.

Crawford, D. A., M. B. Boslough, T. G. Turcano, and A. C. Robinson, The

impact of periodic comet Shoemaker-Levy 9 on Jupiter, *Int. J. Impact Eng.*, *17*, 253–262, 1995.
Crowell, J. C., Ice ages recorded on Gondwanan continents, *Trans. Geol. Soc. S. Afr.*, *18*, 238–262, 1983.
Cuzzi, J. N., Planetary ring systems, *Rev. Geophys.*, *21*, 173–1861, 1983.
Cuzzi, J. N., and P. R. Estrada, Compositional evolution of Saturn's rings due to meteoroid bombardment, *Icarus*, *32*, 1–35, 1998.
D'Hondt, S., M. E. Q. Pilson, H. Sigurdsson, A. K. Hanson, and S. Carey, Surface-water acidification and extinction at the Cretaceous-Tertiary boundary, *Geology*, *22*, 983–986, 1994.
Endal, A. S., Evolutional variations of solar luminosity, in *Variations of the Solar Constant*, *NASA Conf. Publ.*, *2191*, 175–183, 1981.
Fredricksen, N. O., Sporomorph biostratigraphy, floral changes, and paleoclimatology, in *Eocene and Earliest Oligocene of the Eastern Gulf Coast*, *U.S. Geol. Surv. Prof. Pap.*, *1448*, 1–68, 1988.
Ganapathy, R., Evidence for a major meteorite impact on the Earth 34 million years ago: Implication for Eocene extinctions, *Science*, *216*, 885–886, 1982.
Glass, B. P., and P. A. Zwart, North American tektites in deep-sea drilling project cores from the Caribbean Sea and the Gulf of Mexico, *Geol. Soc. Am. Bull.*, *90*, 595–602, 1979.
Hildebrand, A. R., G. T. Penfield, D. A. Kring, M. Pilkington, A. Camargo, Z. S. B. Jacobson, and W. B. Boynton, Chicxculub Crater: A possible Cretaceous/Tertiary impact crater on the Yucatan Peninsula, Mexico, *Geology*, *19*, 867–871, 1991.
Hoffman, P. F., A. J. Kaufman, G. P. Halverson, and D. P. Schrag, A Neoproterozoic snowball Earth, *Science*, *281*, 1342–1346, 1998.
Ivany, L. C., W. P. Patterson, and K. C. Lohmann, Cooler winters as a possible cause of mass extinctions at the Eocene/Oligocene boundary, *Nature*, *407*, 887–890, 2000.
King, E. A., Late Eocene rings around the Earth?, *Nature*, *288*, 103–104, 1980.
Kirschvink, J. L., Late Proterozoic low-latitude global glaciation: The snowball Earth, in *The Proterozoic Biosphere*, edited by J. W. Schopf and C. Klein, pp. 51–52, Cambridge Univ. Press, New York, 1992.
Koeberl, C., W. Poag, W. U. Reimold, and D. Brandt, Impact origin of the Chesapeake Bay structure and the source of the North American tektites, *Science*, *271*, 1263–1266, 1996.
McLaren, D. J., and W. D. Goodfellow, Geological and biological consequences of giant impacts, *Annu. Rev. Earth Planet. Sci.*, *18*, 123–171, 1990.
Melosh, H. J., *Impact Cratering*: *A Geologic Process*, *Oxford Monogr. Geol. Geophys. Ser.*, vol. 11, 245 pp., Oxford Univ. Press, New York, 1989.
Mukhopadhyay, S., K. A. Farley, and A. Montanari, A short duration of the Cretaceous-Tertiary boundary event: Evidence from extraterrestrial helium-3, *Science*, *291*, 1952–1955, 2001.
Oboh, F. E., C. A. Jaramillo, and L. M. Reeves-Morris, Late Eocene–early Oligocene paleofloristic patterns in southern Mississippi and Alabama, U.S. Gulf Coast, *Rev. Paleobot. Palynol.*, *91*, 23–34, 1996.
O'Keefe, J. A., The terminal Eocene event: Formation of a ring system around the Earth?, *Nature*, *285*, 309–311, 1980a.
O'Keefe, J. A., Late Eocene rings around the Earth?, Reply, *Nature*, *288*, 104, 1980b.
O'Keefe, J. A., The terminal Cretaceous event: Circumterrestrial rings of tektite glass particles?, *Cretaceous Res.*, *6*, 261–269, 1985.
O'Keefe, J. D., and T. J. Ahrens, Oblique impact: A process for obtaining meteorite samples from other planets, *Science*, *234*, 346–349, 1986.
Pollack, J. B., O. B. Toon, T. P. Ackerman, C. P. McKay, and R. P. Turco, Environmental effects of an impact-generated dust cloud: Implications for the Cretaceous-Tertiary extinctions, *Science*, *219*, 247–249, 1983.
Pollard, D., and S. L. Thompson, Climate and ice-sheet mass balance at the Last Glacial Maximum from the GENESIS version 2 global climate model, *Quat. Sci. Rev.*, *16*, 841–863, 1997.
Prinn, R. G., and B. Fegley, Bolide impacts, acid rain, and biospheric traumas at the Cretaceous-Tertiary boundary, *Earth Planet. Sci. Lett.*, *83*, 1–15, 1987.
Rampino, M. R., and R. B. Stothers, Flood basalt volcanism during the last 250 million years, *Science*, *241*, 663–668, 1988.
Raup, D. M., and J. J. Sepkoski, Periodic extinction of families and genera, *Science*, *231*, 833–836, 1986.
Rea, D. K., M. Leinen, and T. R. Janecek, Geologic approach to the long-term history of atmospheric circulation, *Science*, *227*, 721–725, 1985.
Rodwell, M. J., and B. J. Hoskins, Subtropical anticyclones and summer monsoons, *J. Clim.*, *14*, 3192–3211, 2001.
Schultz, P. H., and D. E. Gault, Prolonged global catastrophes from oblique impacts, in *Global Catastrophes in Earth History: An Interdisciplinary Conference on Impacts, Volcanism, and Mass Mortality*, edited by V. L. Sharpton and P. D. Ward, *Spec. Pap. Geol. Soc. Am.*, *247*, 239–261, 1990.
Schultz, P. H., M. Zarate, W. Hames, C. Camilión, and J. King, A 3.3-Ma impact in Argentina and possible consequences, *Science*, *282*, 2061–2063, 1998.
Seyfert, C. K., and L. A. Sirkin, *Earth History and Plate Tectonics*, HarperCollins, New York, 1979.
Shoemaker, E. M., Asteroid and comet bombardment of the Earth, *Annu. Rev. Earth Planet. Sci.*, *11*, 461–494, 1983.
Shoemaker, E., C. S. Shoemaker, and R. F. Wolfe, Asteroid and comet flux in the neighborhood of the Earth, in *Global Catastrophes in Earth History: An Interdisciplinary Conference on Impacts, Volcanism and Mass Mortality, Houston, Texas*, *Contrib. 673*, pp. 174–175, Lunar Planet. Inst., Houston, Tex., 1988.
Sigurdsson, H., S. D'Hondt, and S. Carey, The impact of the Cretaceous-Tertiary bolide on evaporite terrane and generation of major sulfuric-acid aerosol, *Earth Planet. Sci. Lett.*, *109*, 543–559, 1992.
Spray, J. G., S. P. Kelley, and D. B. Rowley, Evidence for a late Triassic multiple impact event on Earth, *Nature*, *392*, 171–173, 1998.
Thompson, S. L., and D. Pollard, Greenland and Antarctic mass balances for present and doubled atmospheric CO_2 from the GENESIS version 2 global climate model, *J. Clim.*, *8*, 1104–1121, 1997.
Toon, O. B., J. B. Pollack, T. P. Ackerman, R. P. Turco, and C. P. McKay, Evolution of an impact-generated dust cloud and its effects on the atmosphere, in *Geological Implications of Impacts of Large Asteroids and Comets on the Earth*, edited by L. T. Lilver and P. H. Schulz, *Spec. Pap. Geol. Soc. Am.*, *190*, 187–200, 1982.
Toon, O. B., K. Zahnle, D. Morrison, R. P. Turco, and C. Covey, Environmental perturbations caused by the impacts of asteroids and comets, *Rev. Geophys.*, *35*, 41–78, 1997.
Vonhof, H. B., and J. Smit, Late Eocene microkrystites at Maud Rise (Ocean Drilling Project Hole 689B, Southern Ocean) suggest a global extension of the approximately 35.5 Ma Pacific impact ejecta strewn field, *Meteoritics Planet. Sci.*, *34*, 747–755, 1999.
Vonhof, H. B., J. Smit, H. Brinkhuis, A. Montanari, and A. J. Nederbragt, Global cooling accelerated by early late Eocene impacts?, *Geology*, *28*, 687–690, 2000.
Wei, W. C., How many impact-generated microspherule layers in the upper Eocene?, *Palaeogeogr. Palaeoclimatol. Palaeoecol.*, *114*, 101–110, 1995.
Williams, G. E., Acraman: A major impact structure from the Neoproterozoic of Australia, in *Large Meteorite Impacts and Planetary Evolution*, edited by B. O. Dressler, R. A. F. Grieve, and V. L. Sharpton, *Spec. Pap. Geol. Soc. Am.*, *293*, 209–224, 1994.
Wolfe, J. A., A paleobotanical interpretation of Tertiary climates in the Northern Hemisphere, *Am. Sci.*, *66*, 694–703, 1978.
Zachos, J. C., J. R. Breza, and S. W. Wise, Early Oligocene ice-sheet expansion on Antarctica: Stable isotope and sedimentological evidence from Kerguelen Plateau, southern Indian Ocean, *Geology*, *20*, 569–573, 1992.
Zachos, J. D., L. D. Stott, and K. C. Lohmann, Evolution of early Cenozoic marine temperatures, *Paleoceanography*, *9*, 353–387, 1994.

P. J. Fawcett, Department of Earth and Planetary Sciences, University of New Mexico, 220 Northrop Hall, Albuquerque, NM 87131, USA. (fawcett@unm.edu)

M. B. E. Boslough, Sandia National Laboratories, P.O. Box 5800, Mail Stop 0318, Albuquerque, NM 87185-0318, USA.